Indian Journal of Geo Marine Sciences
Vol. 48 (07), July 2019, pp. 1154-1163

MPI application of 3D hydroelasticity on a barge deployed above the uneven seabed

Ye Lu[1*], Zhan Xu[2], Ye Zhou[1], Jinxiu Xu[2], & Chao Tian[1]
[1]China Ship Scientific Research Center, Wuxi 214082, China
[2]Jiangnan Institute of Computing Technology, Wuxi 214083, China
*[E-mail: luye@cssrc.com.cn]

Nowadays, some floating structures with simple shapes such as barges near the reefs can be deployed as support bases. Unlike the open sea, the greatest feature of the marine environment near the island is the non-uniform complex seabed. In this paper, the hydroelastic analysis method with variable water depths is used to calculate the seakeeping of the floating structures, considering the uneven seabed as the boundary condition. Based on the three-dimensional hydroelasticity theory, the hydroelastic motion and response analysis of the barge is studied, coupled with parallel codes due to a lot of equations caused by the meshes. Considering different water depths and the complex bathymetry, the motion and loads of barge structures have been compared. The design wave parameters have been confirmed by the short-term forecast extreme results, and the whole stress distribution of barge structures near the reef has been shown plus modal stress by model summation. At last, strength evaluation of barge indicates that the effect of inhomogeneous seabed plays a large role in the arrangement of the barge near reefs and parallel calculations save the CPU time.

[Keywords: MPI; Parallel Calculation; 3D Hydroelasticity; Uneven Seabed]

Introduction

It is well known that to reasonably predict the responses of the floating structures in the complex and variable environments plays a significant role in the safety of marine structures. Especially, the bathymetry under water is always uneven and complicated. Even the commercial software, such as AQWA and SESAM, cannot calculate motions and responses of the barge under the non-uniform water depth state. In traditional hydrodynamic analysis, bathymetry is deemed to be uniform. However, the effect of the uneven seabed needs to be considered to obtain realistic status. In fact, the complex varying seabed in the water has played a crucial role in the motion and response assessment of the floating structures. Therefore, wave load prediction and structural safety valuation of the ships must be considered in the practical sea conditions.

The theory of three-dimensional (3D) linear hydroelasticity has been proposed by Bishop, Price and Wu[1] and the 3D hydroelastic analysis is already mature in the case of infinite and uniform water depth. The influence of non-uniform seabed has been investigated by many scholars, beginning with simple submersible shapes. For example, a semi-cylindrical structure of 150 m length and 4 m radius in uniform 6 m water depth, has been examined by Dewi et al[2]. Athanassoulis and Belibassakis[3, 4] calculated the two-dimensional (2D) hydroelastic characteristics of an elastic thin plate in shallow water with uneven seabed, while Gerostathis et al[5] studied its 3D characteristics. Adrianov and Hermans[6] assessed the influence of various parameters, such as wavelength and wave direction, on the 2D hydroelasticity of very large floating structures (VLFS) in infinite and shallow waters. Sun et al[7], Lv et al[8] and Song et al[9] carried out model tests of VLFS considering the impact of the underwater bathymetry in regular and irregular waves. The uneven seabed is modelled using a variety of sand dunes of cylindrical and elliptical form, in the bottom of the wave basin. Kyoung et al[10] designed four different seabed arrangements to calculate the hydroelastic effects of very large floating bodies. Buchner[11] studied the influence of the seabed topography on ship motions modelling the seabed as a second fixed body. He discussed the importance of having sloping boundaries for this second body rather than vertical walls. Considering the model by Buchner[11], the necessity for using sloping boundaries for the modelled seabed terrain was verified by Ferreira et al[12]. Hauteclocque et al[13] also assumed that the seabed topography is modelled as a second body

fixed in the hydrodynamic analysis and obtained more accurate results of the motions and responses of ships. Beside the ships, Utsunomiya et al[14] compared the hydroelastic responses of a box-type VLFS in uniform seabed, a seabed with 1/75 slope and a seabed with variable depth. In addition, Pinkster[15] proposed a simplified method for the hydrodynamic calculation of single-slope submarine terrain boundary, suitable when the mooring of multiple ships near the dock can be divided into multiple areas. The studies, as can be seen, have all used simple shapes for the bathymetry rather than more realistic seabed topography. In fact, the uneven seabed is so complicated to affect marine surface and underwater vehicles investigated by Xiang et al[16,17] and Yu et al[18], and resulting inevitable uncertainties need to be risk analysis[19,20].

Four decades after its inception, the software THAFTS (Three-dimension Hydroelastic Analysis of Floating and Translating Structures) has proved to be a powerful tool for predicting wave-induced motions and loads of floating structures and validated by full-scale measurements and model tests. Considering non-uniform environmental conditions, Wu et al[21,22] and Tian et al[23,24] have further developed the 3D linear hydroelasticity of large-scale floating bodies to account for the wave inhomogeneity, the variable water depth and the multi-module fluid-structures interactions. Li et al[25] investigated the dynamic behaviour of a VLFS in the relatively flat sea region in the middle of a lagoon surrounded by reefs. Yang et al[26] and Lu et al[27] used the same method to examine the motions and loads of the floating structures in non-uniform water depth and near-island reef environment and pointed out that the design load prediction considering the complexity of the seabed topography was important. These results were obtained using parallel computing in conjunction with the Message Passing Interface (MPI) on the "Sunway TaihuLight" supercomputer.

In this paper, the 3D hydroelastic analysis software THAFTS with the parallel computing method of floating structures in uneven seabed is demonstrated using a stationary barge as an example. The seabed is modelled as the second fixed body to solve the equations of motions of the stationary barge structure in this complex environment. Two cases of water depth are considered, namely, 30 m and 10 m. For each of these cases, the seabed is modelled as uniform using the relevant no flow condition at the seabed, and as non-uniform using the second fixed body. The predicted responses include heave and pitch motions and amidships vertical bending moment in regular head waves. Furthermore, the same method is applied using an Equivalent Design Wave (EDW) and illustrating direct stress distribution on the barge.

Method

Brief description of the 3D linear hydroelasticity theory

The hydroelastic analysis of the barge is defined in a Cartesian coordinate system *Oxyz*, with *x*-axis positive to bow, *x*-*y* plane on the undisturbed water surface, *z*-axis pointing upwards and passing through the centre of gravity of the barge. Introducing the principal coordinates $p_r(t)(r=1,2,\cdots,m)$, the displacement $\vec{u}=(u,v,w)$ of the barge is expressed as a summation over the principal modes $\vec{u}_r=(u_r,v_r,w_r)(r=1,2,\cdots,m)$ of the floating structure in vacuo, namely

$$\vec{u}=\sum_{r=1}^{m}\vec{u}_r p_r(t) \tag{1}$$

In this equation r=1, 2, …6, correspond to rigid body motions of surge, sway, heave, roll, pitch and yaw, respectively and *m* denotes the total number of principal modes allowed in the analysis. The generalized equations of motion are represented in terms of p_r in the matrix form as follows:

$$[a+A]\{\ddot{p}\}+[b+B]\{\dot{p}\}+[c+C]\{p\}=\{\Xi(t)\} \tag{2}$$

where $[a]$, $[b]$ and $[c]$ are the generalized mass, structural damping and stiffness matrices of the dry structure and $[A]$, $[B]$ and $[C]$ are the generalized added inertia, hydrodynamic damping and fluid restoring matrices, respectively. $\{p\}$ represents the principal coordinate vector and $\{\Xi(t)\}$ is the generalized wave force vector, containing both incident wave and wave diffraction contributions.

The potentials Φ comprise the incident potential $\phi_I(t)$, diffraction potential $\phi_D(t)$ and radiation potential $\phi_R(t)=\sum_{r=1}^{m}\varphi_r p_r(t)$. All potentials satisfy Laplace's equation and the free surface, seabed, and far-field boundary conditions. The pulsation source Green's function is used for the radiation potentials.

The principal coordinates are obtained in regular waves (frequency domain analysis) and the deformations and internal forces, such as bending

moments and stresses, are obtained using modal summation. For instance, the vertical bending moment about *y*-axis at a cross-section along the structure is

$$M_y = \sum_{r=7}^{m} M_{yr} p_r(t) \tag{3}$$

and the longitudinal direct stress at a defined point (x, y, z) on the section is

$$\sigma_x = \sum_{r=7}^{m} \sigma_{xr} p_r(t) \tag{4}$$

In these equations, σ_{xr} and M_{yr}, represent the modal longitudinal direct stress and modal vertical bending moment for the *r* th mode shape.

When a floating structure is deployed in shallow water, the encountered wave conditions and the structural responses may be greatly influenced by the varied seabed topography. In such a complicated geographic environment, the characteristics of wave evolution must be clarified, and the corresponding hydroelastic analysis approaches must be developed.

When the barge is deployed in shallow water close to the island, the complex seabed can be represented as a fixed boundary. To account for the influence on the diffraction and radiation, the boundary conditions on the non-uniform seabed, represented by the second fixed body, becomes:

$$\frac{\partial \phi_D}{\partial n}\Big|_{z=-h(x,y)} = 0, \tag{5}$$

$$\frac{\partial \phi_R}{\partial n}\Big|_{z=-h(x,y)} = 0, \tag{6}$$

Equations (5, 6), as can be seen, apply to variable water depth appropriate to the uneven seabed topography.

Multi-parameter parallelization

In addition to the complex shape of the floating structure, the fluid domain contains a non-uniform shallow water environment. Therefore, many panels to discretise floating structure-fluid interface and non-uniform seabed are required. Usually, a larger extent of the seabed needs to be modelled by comparison to the floating structure. Furthermore, as the seabed does not possess port/starboard symmetry as typical conventional ships, the number of panels is much larger than those of the floating body, thus increasing the calculation effort. Therefore, the analysis process is very slow when using a serial code, exacerbated by the number of distortion modes included and wave frequencies for which the analysis is carried out.

Accordingly, the MPI and multi-level parallel programming model are used, focusing at the wet panels, the wave frequencies and so on, rather than the existing serial THAFTS program. The calculations were performed on the "Sunway TaihuLight", which is ranked 3rd in the current TOP500 supercomputer list (Top position in 06/2016, 11/2016, 06/2017 and 11/2017). This is a system developed by China's National Research Center of Parallel Computer Engineering & Technology (NRCPC) and installed at the National Supercomputing Center in Wuxi. Using the aforementioned high-performance computing facilities, the calculation times decreased significantly for the 3D linear hydroelastic motions and structural dynamic responses of the barge with the non-uniform seabed conditions in the near-island environment.

Frequency domain parallel improvement: To pursue higher communication performance, select the front N-1 processors to deal with the same size of data while the last processor to deal with the remaining data way to divide the data. When the number of processes is small, the drawbacks of this partitioning method are not exposed. However, as the number of processes increases to a certain scale, the number of data such as mesh numbers that should be allocated in the last process according to the original allocation mode becomes negative, resulting in operating procedures being error such as MPI_reduce. Therefore, the data distribution mode is replaced by a common way, that is, mod function is performed on the mesh numbers by using the process number. The process of the rank (myid) being less than the above results of data distribution equal to quotient plus one due to the remainder, which can ensure the correctness of the operation of the messages, to some extent, and improve the balance of process loads.

Performance optimisation: After the get K function being picked outside of multiple loops and put in a finite water depth computation according to the actual calculation, the performance of calling the function module is improved by 100 times, as shown in Table 1.

In addition, the procedure of solving a specific function takes a long time to solve this problem. In response to this feature, the Blas library and the

Table 1 — Comparison of the getK function by optimisation

Original (sec)	Optimisation (sec)	Improvement rate
233.72	2.17	107.37

Lapack library that are processed by the many-core are invoked to increase the computational efficiency of the hot spot function in a single frequency calculation by about 20 times as given in Table 2.

Structural and Hydrodynamic Modelling

Structural model

The principal particulars of the barge are shown in Table 3. A typical fully loaded condition is selected for the analysis. The 3D structural model, as shown in Figure 1, was generated by suitable beam and shell finite elements. A total of 70029 elements were used for the whole barge structure, in the MSC.Patran software, to model major structural components, such as deck, side shell, double bottom, transverse bulkheads, longitudinal girders, superstructures, etc.

The Lanczos method was selected to obtain the eigenvalues and eigenvectors. The first four natural frequencies and mode shapes of the vessel freely vibrating in vacuo are shown in Figure 2. A total of 30 distortion modes was included in the analysis, i.e., m=36.

The vehicle ramp, situated near the fore quarter and the superstructure disrupt the port starboard symmetry, as can be seen in Figure 1. However, as can be seen from Figure 2, this small asymmetry has very little effect on the symmetric nature of the 2-node or 3-node vertical bending modes or the antisymmetry of the 1-node twisting and 2-node horizontal bending modes. Therefore, the conventional definition for port-starboard symmetric structures is still used. Accordingly, the principal mode shapes of this barge were defined as symmetric (2-node and 3-node vertical bending) and antisymmetric (1-node torsion and 2-node horizontal bending). The coupling between torsion and horizontal bending is relatively small and inherent in the 3D finite element model.

Table 2 — Comparison of CPU times in single frequency before and after optimisation

Original (sec)	Optimisation (sec)	Improvement rate
20819.62	934.49	22.28

Table 3 — Principal particulars of the barge

Characteristics	Unit	Value
Length between perpendiculars	m	100.0
Breadth moulded	m	25.0
Draught	m	2.7
Displacement	t	6479.3
Longitudinal centre of gravity from A.P.	m	50.0
Vertical centre of gravity from B.L.	m	4.43
Inertia moment about *x*-axis	$kg \cdot m^2$	1.967×10^8
Inertia moment about *y*-axis	$kg \cdot m^2$	5.403×10^9
Inertia moment about *z*-axis	$kg \cdot m^2$	5.503×10^9

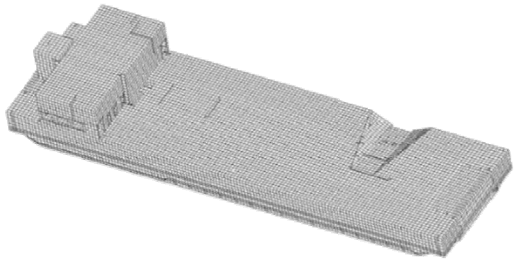

Fig. 1 — Structural FE model of the barge comprising 70029 elements in total.

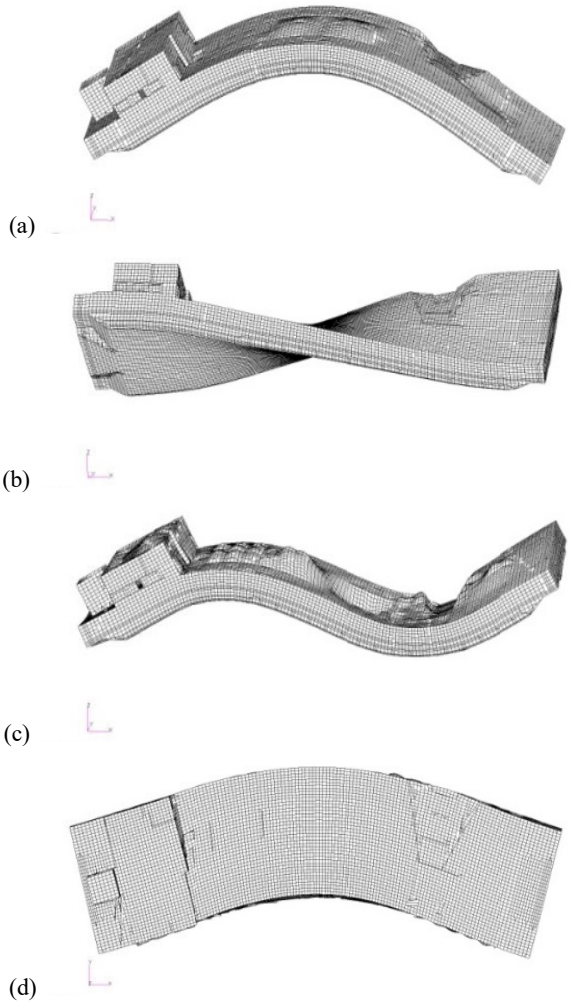

Fig. 2 — The first four flexural mode shapes of the barge and corresponding nature frequencies: (a) 2-node vertical bending (r=7), 2.038Hz; (b) 1-node torsion (r=8), 3.024Hz; (c) 3-node vertical bending (r=9), 4.475Hz; (d) 2-node horizontal bending (r=10), 5.141Hz.

Hydrodynamic model

Located in shallow water near a reef, the seabed is non-uniform. To ascertain the effects of varying bathymetry on the dynamic behaviour of the floating barge, two models of the environment were used: (i) Uniform seabed and (ii) Seabed with varying topography modelled as a second fixed body. For the latter, only the local terrain range was modelled, under the assumption that this is the seabed region that will affect the motions and loads of the floating body. This also reduces the amount of calculations performed. The selected seabed has length of 200 m and width of 120 m, along the x and y axes, respectively as per the floating barge. The topography of the seabed is completely submerged with the fixed body boundaries sloping smoothly. The seabed topography corresponds to real seabed data near reefs. Two depths are considered corresponding to vertical distances between the seabed and the barge centre of gravity of 30 m and 10 m. There are 3476 four-cornered or three-cornered wet panels on the barge (whole of the barge) wetted interface. There are 9792 panels on the seabed as shown in Figure 3, nearly three times of the floating body. It should be noted that the normal points out to the flow both for the barge and the second body representing the seabed. The hydrodynamic model of the barge/seabed system with complicated terrain is shown in Figure 3.

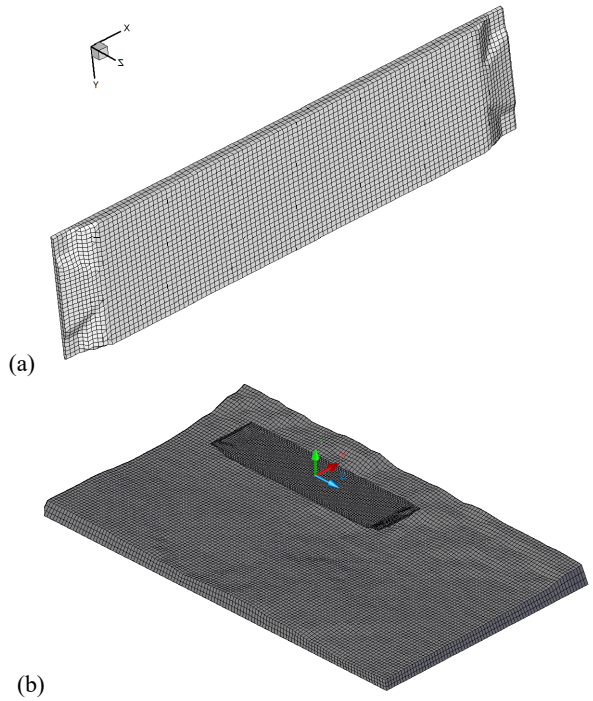

Fig. 3 — Hydrodynamic model: (a) hydrodynamic panels of barge; (b) hydrodynamic panels of barge including bathymetry of seabed

Results and Discussion

Influence of water depth and bathymetry

For the analysis in this paper the barge is stationary in regular head waves. Using the serial code in a typical workstation requires 6.5 hours to complete the calculations for one wave frequency. On the other hand, the same calculation is carried out in 100 s CPU time on the supercomputer using parallel computing with MPI.

The typical added mass, damping, exiting forces, heave and pitch motions of the barge in head regular waves of unit amplitude are demonstrated in Figures 4-11, respectively, as a function of the wave frequency ω. The response amplitude operator (RAO) of the amidships vertical bending moment (VBM) of the barge in head waves are represented in Figures 12 and 13. Both uniform and complex seabed topographies are included for 30 m and 10 m water depths.

Considering uniform seabed, heave RAOs show a decrease with decreasing water depth in low wave frequencies. Pitch RAO peaks appear to be unaffected by changes in the uniform water depth. Similar trends for heave and pitch RAOs were observed by Feng et al[28] who investigated the influence of depth using the commercial software WADAM, as well as Buchner's calculations[11]. On the other hand, amidships VBM RAO peaks increase with decreasing uniform water depth. Furthermore, the peak of VBM and pitch RAOs is observed at lower wave frequencies with decreasing uniform water depth. This implies that the conventional ship-wave matching concept in infinite water depth is affected considerably by decreasing water depth.

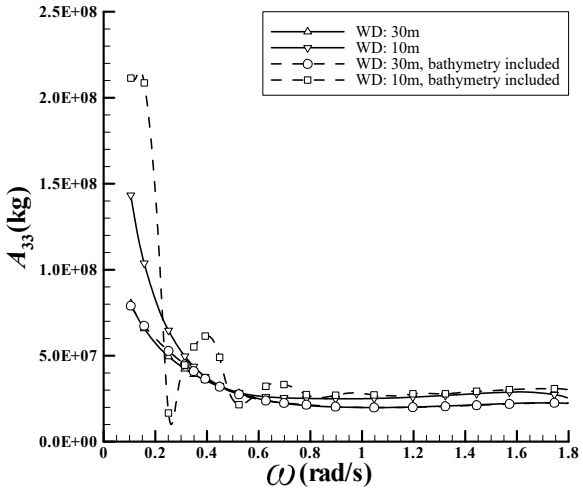

Fig. 4 — Comparison added mass of heave motion at different water depths

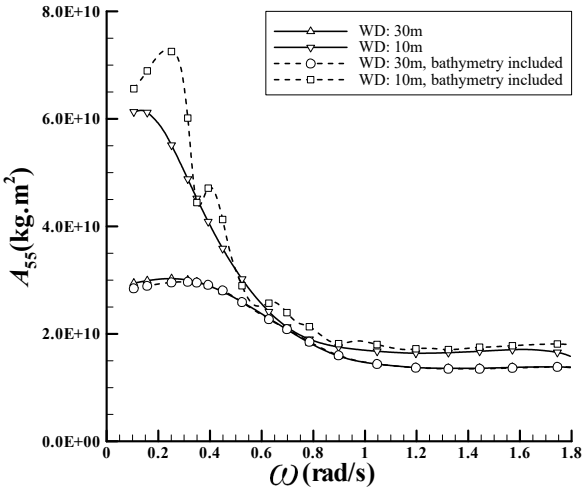

Fig. 5 — Comparison added mass of pitch motion at different water depths

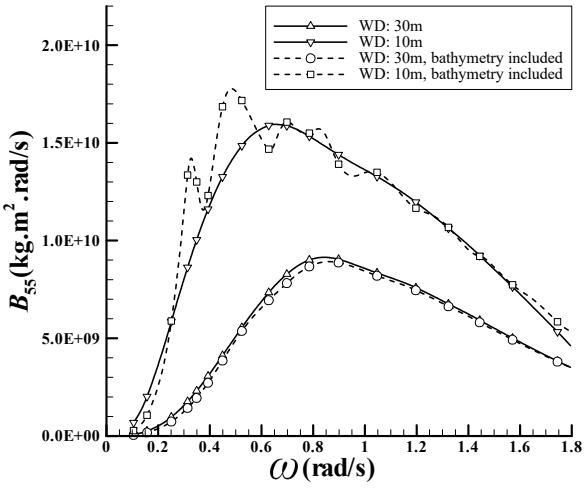

Fig. 7 — Comparison damping of pitch motion at different water depths

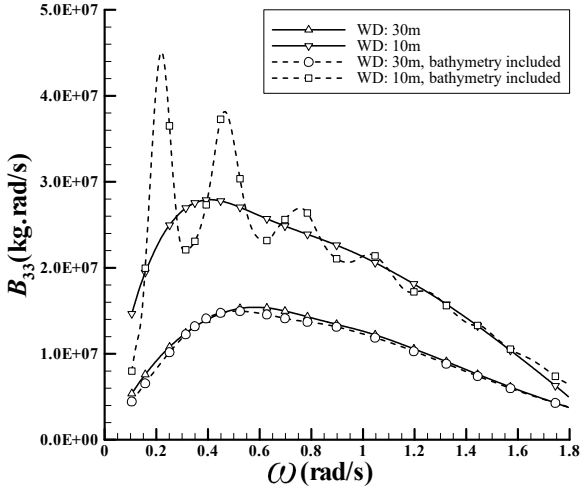

Fig. 6 — Comparison damping of heave motion at different water depths

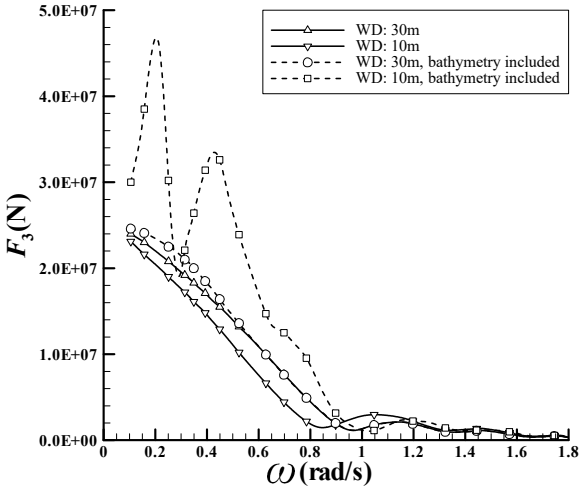

Fig. 8 — Comparison exiting forces of pitch motion at different water depths (in 45°wave direction)

The influence of the non-uniformity of the seabed is dependent on the water depth itself, as can be seen from Figures 10, 11 and 13. For the 30 m water depth, the non-uniformity of the seabed has small influences on heave and pitch RAOs in 45-degree wave direction. This is also true for the amidships VBM RAO, which has a smaller peak for the non-uniform seabed compared to the uniform seabed case. At this depth, the non-uniformity of the terrain does not influence the wave frequency at which pitch and VBM RAOs peak. On the other hand, for the 10 m water depth, significant increases are observed in the heave and pitch RAOs and amidships VBM RAOs, the former almost doubling the heave and pitch RAO peak and the latter showing a nearly 50% increase in the peak value. It should be noted that the numerical predictions by Buchner[11] for 15 m non-uniform water depth also show similar increase in heave and pitch RAOs in relatively low wave frequencies. It is also observed that the non-uniformity of the seabed results in a peak for the heave RAO, albeit at a wave frequency lower than that for the peak pitch RAO. The wave frequencies at which the pitch and amidships VBM RAOs peak also become smaller as a result of the non-uniformity.

Short-term extreme value forecast

According to measured data in the target sea area, the Jonswap wave spectrum is applicable to the limited wind area, namely

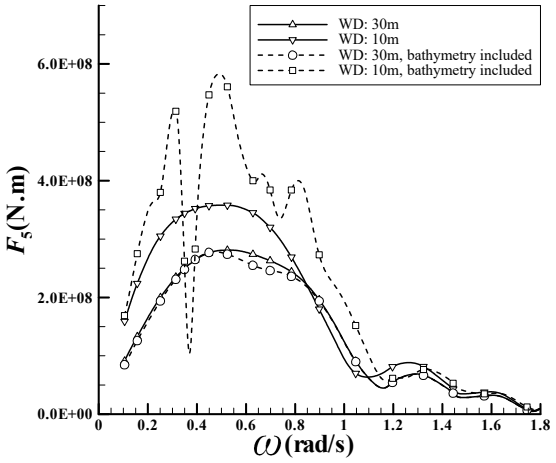

Fig. 9 — Comparison RAOs of pitch motion motion at different water depths (in 45°wave direction)

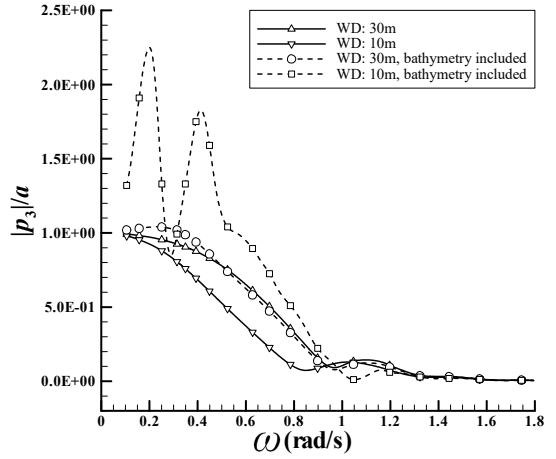

Fig. 10 — Comparison RAOs of pitch motion motion at different water depths (in 45°wave direction)

$$S(\omega)=\alpha g^2\omega^{-5}\exp\left[-\frac{5}{4}\left(\frac{\omega}{\omega_p}\right)^{-4}\right]\gamma^{\exp\left[-0.5\left(\frac{\omega-\omega_p}{\sigma\omega_p}\right)^2\right]} \quad (7)$$

where, the generalized constant of Jonswap spectrum $\alpha=(5/16)\left(H_s^2\omega_p^4/g^2\right)\left[1-0.287\ln(\gamma)\right]$, H_s is the significant wave height, ω and ω_p are the wave and peak frequencies, respectively, and g is the gravitational acceleration. γ is a non-dimensional peak shape parameter which follows a Gaussian distribution with mean value of 2.0, according to the measured statistical data and σ is a numerical parameter, $\sigma=0.07(\omega\le\omega_p)$, $\sigma=0.07(\omega>\omega_p)$.

Although this barge may be subject to a variety of external loads, the wave-induced load is the main part of the external loading and plays a decisive role in the assessment of the longitudinal strength. In this paper,

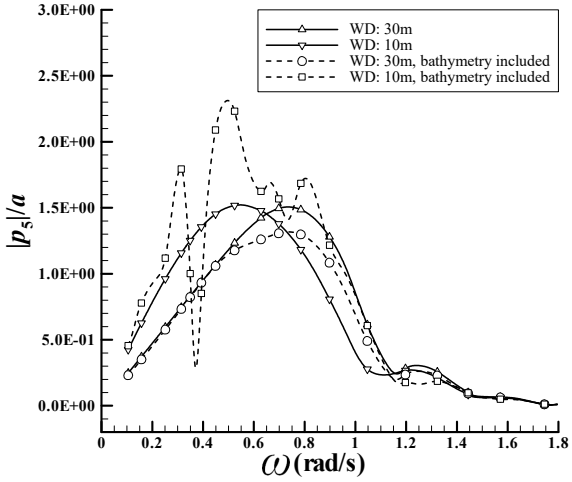

Fig. 11 — Comparison RAOs of pitch motion motion at different water depths (in 45°wave direction)

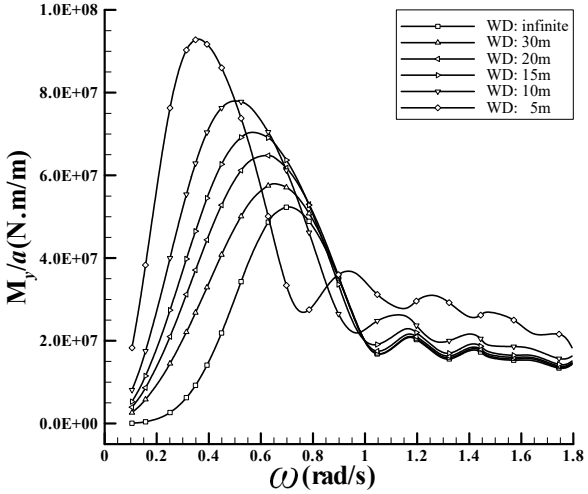

Fig. 12 — Comparison of RAOs of VBM at amidships at different uniform water depths

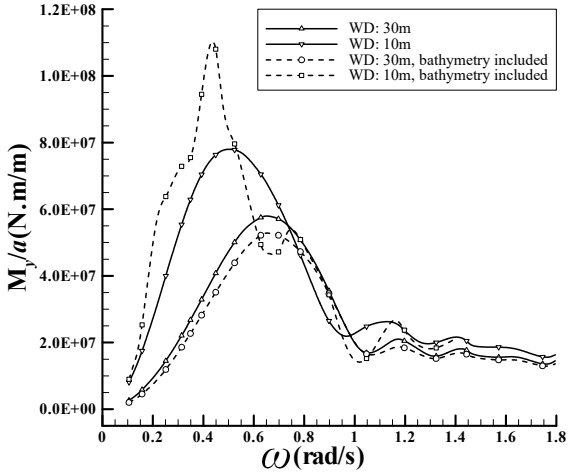

Fig. 13 — Comparison of RAOs of VBM at amidships with uniform and non-uniform bathymetry

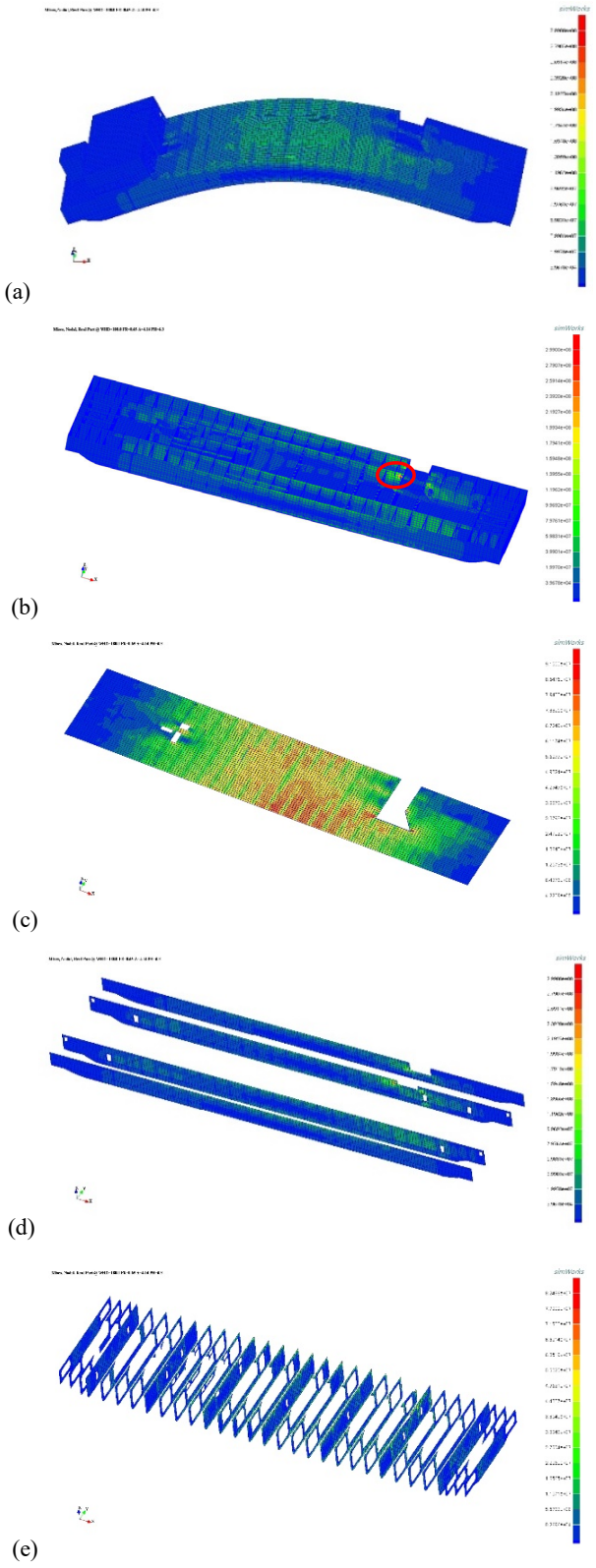

Fig. 14 — Direct stress distribution of the barge in EDW2: (a) the whole structure, (b) the structures under the deck, (c) the deck, (d) the longitudinal bulkheads, (e) the transverse bulkheads.

Table 4 — Equivalent design wave parameters

Sea conditions T_p (s)		7.21	9.08	10.95
RMS[a] VBM at L/2	0º	1.23×10^8	1.69×10^8	1.76×10^8
(N•m)	180º	1.37×10^8	1.76×10^8	1.80×10^8
VBM RAO Peak (N•m)	0º	5.63×10^7		
	180º	5.69×10^7		
EDW1				
Wave amplitude (m)		4.08		
Wave period (s)		9.662		
Wave direction (º)		180		
Phase (º)		0.2		
RMS VSF at L/4 (N)	0º	3.24×10^6	4.67×10^6	4.95×10^6
	180º	4.30×10^6	5.26×10^6	5.30×10^6
VSF RAO Peak (N)	0º	1.60×10^6		
	180º	1.65×10^6		
EDW2				
Wave amplitude(m)		4.14		
Wave period (s)		9.662		
Wave direction (º)		180		
Phase (º)		6.3		
RMS VSF at 3L/4 (N)	0º	4.54×10^6	5.86×10^6	5.99×10^6
	180º	4.11×10^6	4.87×10^6	5.86×10^6
VSF RAO Peak (N)	0º	1.90×10^6		
	180º	1.88×10^6		
EDW3				
Wave amplitude(m)		4.07		
Wave period (s)		9.662		
Wave direction (º)		0		
Phase (º)		-2.3		
Root Mean Square (RMS)				

the wave load is calculated by the equivalent design wave method.

The design parameters of the barge for three peak periods T_p are given in Table 4, for significant wave height H_s=4m. Head and following waves are denoted by 180° and 0°, respectively. The peak RAO of vertical bending moments and shear forces (VSF), amongst different wave directions, always occurred at 0° and 180°; hence, only these two angles are compared in Table 4. The EDW parameters are also provided in Table 4.

Stress distribution

Using the equivalent design wave parameters, the stress analysis of the barge is carried out directly by hydroelastic method. It is not necessary to apply the corresponding external load to the structural model, basically used in the traditional method. A hydroelastic analysis is carried out using the properties of the EDW, in water depth of 30 m with non-uniform seabed, and evaluating the stresses using equation (4).

The results, presented in Figure 14, show that the direct stresses at amidships are larger than other

positions along the barge. In addition, considering EDW2 shear forces, hence shear stresses, at the aft quarter section (L/4) are maximum.

Conclusion

In this paper, the subject of a floating body operating near islands together with non-uniform seabed topography is investigated using 3D linear hydroelasticity. This is an important problem, considering increase in offshore operations and the associated complexity of the seabed.

In the absence of commercial software which can predict the performance of floating marine structures operating near reefs, including varying bathymetry, 3D hydroelastic software THAFTS has been further developed to perform such an analysis.

In this paper, the motions and vertical bending moments of the barge, stationary in head waves, in uniform and non-uniform seabed terrains were compared. Based on these predictions, it is concluded that the influence of the uneven seabed is significant enough to be considered when marine structures are deployed near islands and reefs in shallow water, e.g. of the order of 0.1 L. Further investigations are necessary to understand the influence of the seabed topography on different wave-induced motions and loads, particularly as a function of the amount of non-uniformity in the seabed topography.

Furthermore, the current method, which allows for non-uniformity of seabed, has been applied to an equivalent design wave showing the complexities involved in EDW parameters in terms of bending moments, shear forces and wave direction.

The hydrodynamic models used include complex bathymetry and hence require very large number of panels when modelling the floating body and the seabed, the latter as a second fixed body. Use of the Sunway TaihuLight supercomputer, currently the computing speed being the one of the fastest in the TOP500 list, has significantly improved the CPU time used combined with parallel computing and the MPI method.

Acknowledgment

The work was supported by the Ministry of Science and Technology with the research project (Grant No. 2013CB36100, No. 51809241 and 2017YFB0202702) and the Ministry of Industry and Information Technology with the research project in the field of high-tech ships (2016[22]).

References

1 Bishop, R.E.D., Price, W.G. & Wu, Y.S., A general linear hydroelasticity theory of floating structures moving in a seaway, *Phil Os T R Soc A*, 316(1986) 375-426.

2 Dewi, F.D.E., Liapis, S.I. & Plaut R.H., Three-dimensional analysis of wave attenuation by a submerged, horizontal, bottom-mounted, flexible shell, *Ocean Eng*, 26(1999) 813-839.

3 Athanassoulis, G.A., & Belibassakis, K.A., A novel coupled-mode theory with application to hydroelastic analysis of thick, non-uniform floating bodies over general bathymetry, *P I Mech Eng M- J Eng*, 223(2009) 419-438.

4 Belibassakis, K.A. & Athanassoulis, G.A., A coupled-mode model for the hydroelastic analysis of large floating bodies over variable bathymetry regions, *J Fluid Mech*, 531(2005) 221-249.

5 Gerostathis, T.P. Belibassakis, K.A. & Athanassoulis, G.A., 3D hydroelastic analysis of very large floating bodies over variable bathymetry regions, *Journal of Ocean Engineering and Marine Energy*, (2016) 159-175.

6 Andrianov, A.I. & Hermans, A.J., The influence of water depth on the hydroelastic response of a very large floating platform, *Mar Struct*, 16(2003) 355-371.

7 Sun, H., Cui, W.C. & Liu, Y.Z., Hydroelastic response of very large floating Structures over 2D variable bottom, *Journal of Shanghai Jiaotong University*, 37(2003) 1172-1175.

8 Lv, H.N., Yang, J.M. & Yao, M.W., Experimental research of the hydroelastic response of box-typed VLFS in non-uniform sea environment, *The Ocean Engineering*, 22(2004) 1-8.

9 Song, H., Tao, L.B., Cui, W.C. & Liu, Y.Z., Hydroelastic response of VLFS on uneven sea bottom, *ASME 2005 24th International Conference on Offshore Mechanics and Arctic Engineering*, OMAE 2005-67557.

10 Kyoung, J.H., S.Y. Hong, Kim, B.W. & Cho, S.K., Hydroelastic response of a very large floating structure over a variable bottom topography, *Ocean Eng*, 32(2005) 2040-2052.

11 Buchner, B., The motions of a ship on a sloped seabed, *ASME 2006 25th International Conference on Offshore Mechanics and Arctic Engineering*, OMAE2006-92321.

12 Ferreira, M.D. & Newman, J.N., Diffraction effects and ship motions on an artificial seabed, *24th International Workshop on Water Waves and Floating Bodies*, 2009.

13 Hauteclocque, G.D., Rezende, F., Giorgiutti, Y. & Chen, X.B., Wave kinematics and seakeeping calculation with varying bathymetry, *ASME 2009 28th International Conference on Ocean, Offshore and Arctic Engineering*, OMAE2009-79517.

14 Utsunomiya, T., Watanabe, E. Noguchi, T., Yamamoto, S., Kusaka, T. & Ogamo, T., Hydroelastic analysis of a hybrid-type VLFS in water of variable depth, *ASME 2008 27th International Conference on Offshore Mechanics and Arctic Engineering*, OMAE 2008-57180.

15 Pinkster, J.A., A multi-domain approach in 3-d diffraction calculations, *ASME 2011 30th International Conference on Ocean, Offshore and Arctic Engineering*, OMAE2011-49414.

16 Xiang, X.B., Yu, C.Y., Lapierre, L., Zhang, J.L. & Zhang, Q. Survey on fuzzy-logic-based guidance and control of marine surface vehicles and underwater vehicles. *Int. J. Fuzzy Syst*, 20(2018) 572-586.

17 Chu, Z.Z., Xiang, X.B., Zhu D.Q., Luo, C.M., Xie, D., Adaptive Fuzzy Sliding Mode Diving Control for Autonomous Underwater Vehicle with Input Constraint. *Int J Fuzzy Syst*, 20(2018) 1460-1469.

18 Yu, C.Y., Xiang, X.B., Lapierre, L. & Zhang, Q., Robust magnetic tracking of subsea cable by AUV in the presence of sensor noise and ocean currents. *IEEE J Oceanic Eng*, 43(2018) 311-322.

19 Zhang, Q., Zhang, J.L., Chemori, A., Xiang, X B., Virtual Submerged Floating Operational System for Robotic Manipulation. *Complexity*, (2018) 1-18.

20 Yu, C.Y., Xiang, X.B., Wilson, P.A., Zhang, Q., Guidance-error-based Robust Fuzzy Adaptive Control for Bottom Following of a Flight-style AUV with Saturated Actuator Dynamics, *IEEE Trans Cybern*, (2019) 1-13.

21 Wu, Y.S., Zou, M.S., Tian, C., Sima, C., Qi, L.B., Ding, J., et al. Theory and applications of coupled fluid-structure interactions of ships in waves and ocean acoustic environment, *J Hydrodyn*, 28(2016) 923-936.

22 Wu, Y.S., Ding, J., Li, Z.W., Ni, X.Y., Wu, X.F. & Tian, C., Hydroelastic responses of vlfs deployed near islands and reefs, *ASME 2017 36th International Conference on Ocean, Offshore and Arctic Engineering*, OMAE2017-62680.

23 Tian, C., Ni, X.Y., Liu, X.L. & Wu, Y.S., Hydroelastic investigation on floating body near islands and reefs, *Proceedings of the 11th International Conference on Hydrodynamics* (ICHD 2014).

24 Tian, C., Ni, X.Y., Ding, J., Yang, P. & Wu, Y.S., Theoretical study on hydroelastic responses of very large floating structures near islands and reefs, *ASME 2014 33rd International Conference on Ocean, Offshore and Arctic Engineering*, OMAE2014-24704.

25 Li, Z.W., Zhang, Z.W., Tian, C. & Ding, J., A study on connector loads of very large floating structures near islands and reefs, *Journal of Ship Mechanics*, 21(2017), 329-338.

26 Yang, P., Gu, X.K., Tian, C., Cheng, X.M. and Ding, J., Numerical study of 3D pulsating source green function of finite water depth, *ASME 2014 33rd International Conference on Ocean, Offshore and Arctic Engineering*, OMAE2014-24703.

27 Lu, Y., Fan, C.Z., Zhang, Z.W. & Tian, C., Hydroelasticity of floating platform near island effected by bathymetry based on THAFTS software, *Journal of Ship Mechanics*, (in press).

28 Feng, Q.D., Hu, J.J., Yang, P. & Zhang, F., Research on damaged ship motion and wave load in finite water, *Journal of Ship Mechanics*, 19(2015) 381-388.